

High-Throughput Screening for Band gap Engineering by Sublattice Mixing of $\text{Cs}_2\text{AgBiCl}_6$ from First-Principles

Deepika Gill, Preeti Bhumla, Manish Kumar, and Saswata Bhattacharya*

Department of Physics, Indian Institute of Technology Delhi, New Delhi, India

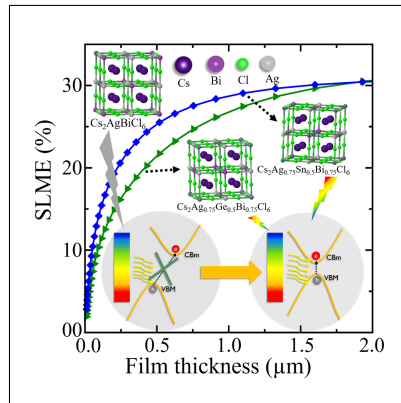
E-mail: saswata@physics.iitd.ac.in[SB]

Phone: +91-11-2659 1359. Fax: +91-11-2658 2037

Abstract

The lead-free double perovskite material (viz. $\text{Cs}_2\text{AgBiCl}_6$) has emerged as an efficient and environmentally friendly alternative to lead halide perovskites. To make $\text{Cs}_2\text{AgBiCl}_6$ optically active in the visible region of solar spectrum, band gap engineering approach has been undertaken. Using $\text{Cs}_2\text{AgBiCl}_6$ as a host, band gap and optical properties of $\text{Cs}_2\text{AgBiCl}_6$ have been modulated by alloying with M(I), M(II), and M(III) cations at Ag-/Bi-sites. Here, we have employed density functional theory (DFT) with suitable exchange-correlation functionals in light of spin-orbit coupling (SOC) to determine the stability, band gap and optical properties of different compositions, that are obtained on Ag-Cl and Bi-Cl sublattices mixing. On analyzing the 64 combinations within $\text{Cs}_2\text{AgBiCl}_6$, we have identified 19 promising configurations having band gap sensitive to solar cell applications. The most suitable configurations with Ge(II) and Sn(II) substitutions have spectroscopic limited maximum efficiency (SLME) of 32.08% and 30.91%, respectively, which are apt for solar cell absorber.

Graphical TOC Entry



Inorganic-organic (IO) hybrid halide perovskites (AM(II)X_3 , $\text{A} = \text{methylammonium (MA}^+)$, formamidinium (FA^+); $\text{M(II)} = \text{Pb}^{2+}$; $\text{X} = \text{Cl}^-$, Br^- , I^-) have brought a huge revolution in the field of photovoltaics.¹⁻³ These alluring materials exhibit high absorption coefficient, long carrier diffusion length, high carrier mobility, low trap density, low manufacturing cost and high defect tolerance.⁴⁻⁷ Starting from 3.8%, their power conversion efficiency (PCE) has risen to 22.7%^{4,8,9} in just a decade. Despite these attainments, the intrinsic instability owing to monovalent organic cation¹⁰ and toxicity of Pb^{11} hinder their large scale commercialization. To address these problems, extensive efforts have been paid to find stable and green alternatives for optoelectronic applications. In the recent years, despite large success of IO hybrid perovskites, researchers are getting back to inorganic perovskites as the former suffers from intrinsic stability. It has been reported that the problem of intrinsic instability can be overcome by replacing organic cation with inorganic cation i.e., Cs^+ . This not only upgrades the thermal stability but also exceeds device's life span.^{12,13} However, in CsPbX_3 , toxic nature of Pb is still a big issue and replacement of Pb with some non-toxic element provides a permanent solution. Also, complete replacement of Pb with elements belonging to the same group like Sn and Ge is not suitable due to their tendency of oxidization from +2 state to +4 state.^{14,15} Considering any other divalent cation in place of Pb results in poor optoelectronic properties owing to their large band gap.^{16,17} Alternatively, without varying the total number of valence electrons, two Pb^{2+} cations can be transmuted by one monovalent (M(I)) and one trivalent (M(III)) cation. It leads to a new configuration i.e., $\text{Cs}_2\text{M(I)M(III)X}_6$,^{18,19} which procures a double perovskite structure. Following this kind of design strategy, a few experimentally reported double perovskites are $\text{Cs}_2\text{AgBiX}_6$ [$\text{X} = \text{Cl}$, Br , I],²⁰⁻²² $\text{Cs}_2\text{AgSbX}_6$,^{23,24} $\text{Cs}_2\text{AgInX}_6$ ^{25,26} and $\text{Cs}_2\text{InM(III)X}_6$ [$\text{M(III)} = \text{Sb}$, Bi].²⁷ However, none of them are ideal for solar cell applications due to the imperfections associated with them. In case of $\text{Cs}_2\text{AgM(III)X}_6$ [$\text{M(III)} = \text{Sb, Bi}$], the large indirect band gap results in poor solar absorption. On the other hand, parity forbidden transition and inevitable conversion of In^{1+} to In^{3+} in $\text{Cs}_2\text{AgInX}_6$ ²⁵ and $\text{Cs}_2\text{InM(III)X}_6$ [$\text{M(III)} = \text{Sb, Bi}$],²⁸ respectively, lead to

degradation of photovoltaic performance.

In this Letter, we present an intensive theoretical study on band gap transmutation of $\text{Cs}_2\text{AgBiCl}_6$ by means of sublattice mixing. The sublattice mixing is done by substituting M(I) at Ag-sites, M(II) at Ag- and Bi-sites simultaneously, and M(III) at Bi-sites in various concentrations for enhancing the optical properties of $\text{Cs}_2\text{AgBiCl}_6$. A high-throughput screening is performed by carrying out the hierarchical computations employing state-of-the-art first-principles based methodologies under the framework of density functional theory (DFT). We start doing a lot of pre-screening of a large number of configurations with DFT using generalized gradient approximation based exchange-correlation (ϵ_{xc}) functional (PBE²⁹) and following that the promising candidate structures are further analyzed using hybrid DFT with HSE06.³⁰ The latter ϵ_{xc} functional helps for more accurate understanding of the excited state properties. Note that in all the above calculations (viz. PBE or HSE06), the effect of spin-orbit coupling (SOC) is always taken into consideration. This is a crucial step to determine the accurate band gap and band-edge positions of these systems due to presence of heavy metal atoms. We have started with 64 sets of different combinations of metals M(I), M(II), and M(III) respectively. Firstly, the structural stability is predicted using the Goldschmidt's tolerance factor and octahedral factor. It is worth noting that structural stability alone is not sufficient for the formation of perovskites. Hence, to validate the material's thermodynamic stability, the enthalpy of decomposition (ΔH_D) is calculated. Then, from ΔH_D and band gap range (which expands the spectral response in visible region), the promising stable double perovskite configurations are identified. Following identification of such potential candidate structures, detailed electronic structure is carried out alongside of computing optical properties. The real and imaginary parts of the dielectric function are analyzed to understand the effect of sublattice mixing in $\text{Cs}_2\text{AgBiCl}_6$ for transmutation of band gap. Subsequently, we determine spectroscopic limited maximum efficiency (SLME) of all the stable configurations that possess direct band gap, to determine efficient solar cell absorber.

Initially, the benchmarking of ϵ_{xc} functional has been performed by calculating the band gap of pristine system viz. $\text{Cs}_2\text{AgBiCl}_6$. The band gap of $\text{Cs}_2\text{AgBiCl}_6$ with PBE ϵ_{xc} functional is 2.06 eV, which is not in agreement with the experimental value of 2.77 eV.³¹ As this system contains heavy metal atom (viz. Bi), the inclusion of SOC becomes important.⁶ However, incorporation of SOC with PBE underestimates the band gap (1.68 eV) further due to splitting of the conduction band minimum (CBm). The latter gets shifted to lower energy toward Fermi-level, whereas the valence band maximum (VBM) remains unaffected (see Figure S1a in Supplementary Information (SI)). On the other hand, to include the self-interaction error of a many-electron system in the expression of ϵ_{xc} functional, advanced hybrid ϵ_{xc} functional viz. HSE06 becomes essential. It gives a band gap of 3.15 eV (without SOC, HSE06 only) and 2.60 eV (with SOC, HSE06+SOC) respectively with default (0.25) Hartree-Fock exchange fraction (α) (see SI Figure S2). On increasing α to 0.30 and 0.35, we have obtained band gaps of 2.79 and 2.99 eV, respectively using HSE06+SOC (see Figure S1 and S2 in SI). Note that using HSE06+SOC w.r.t the experimental value, though the band gap with $\alpha = 0.30$ is more accurate than that of default value (i.e. $\alpha = 0.25$), we still have proceeded with default one for further calculations. This is due to the fact that on alloying with various metals, the value of α can vary from one system to other, and determining the same without experimental results is next to impossible for new configurations. Therefore, we expect, atleast the default α should give a correct trend qualitatively even if the actual numbers may differ marginally as in the case of pristine $\text{Cs}_2\text{AgBiCl}_6$.

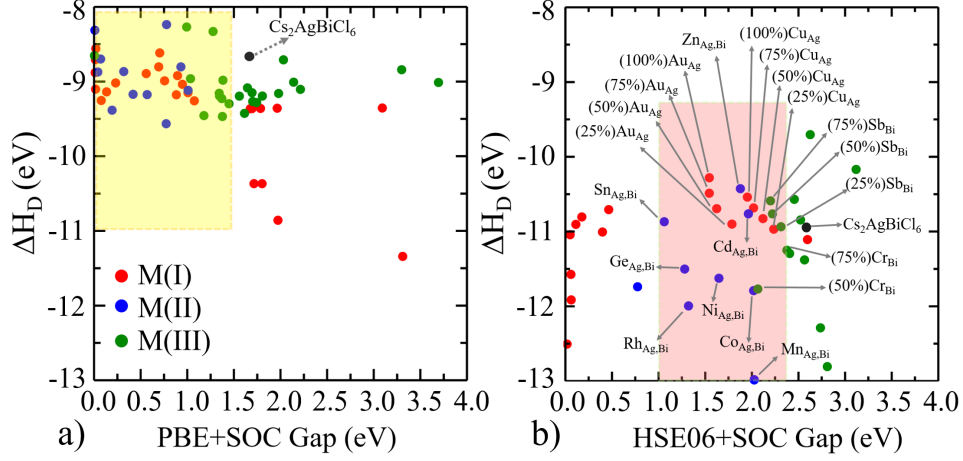


Figure 1: Band gap and ΔH_D using (a) PBE+SOC and (b) HSE06+SOC ϵ_{xc} functionals. (Here, red, blue and green color circular dots correspond to M(I) (e.g., substitution of 25% Au at Ag-site ((25%)Au_{Ag})), M(II) (e.g., substitution of Sn at Ag- and Bi-site simultaneously (Sn_{Ag,Bi})) and M(III) (e.g., substitution of 25% Sb at Bi-site ((25%)Sb_{Bi})), respectively.)

We have started with 64 configurations of double perovskites obtained on mixing the Ag-Cl and Bi-Cl sublattices with M(I) (viz. Au, Cu, In, K, Na, and Ti), M(II) (viz. Cd, Co, Cu, Ge, Mn, Mo, Ni, Sn, V, Zn, and Rh), and M(III) (viz. Cr, Ga, In, Tl, Sb, and Y). Here, we have varied the concentration of the alloying atom viz. 25%, 50%, 75% and 100%. Two fundamental factors need to be satisfied for the stability of double perovskites to exist in high symmetry cubic structure, viz. Goldschmidt's tolerance factor (t)³² and octahedral factor (μ).³³ For structural stability, t should lie between 0.8 and 1.0, and μ should be greater than 0.41.³⁴ To calculate these two fundamental factors for various double perovskite configurations, we have employed a strategy.³⁵ All the selected double perovskite configurations satisfy these stability criteria (see Table S1 in SI). After structural stability, we have also determined the thermodynamic stability by calculating ΔH_D for decomposition of different conformers (obtained after alloying with M(I), M(II), and M(III)) into binary compounds, using following equations:

$$\begin{aligned} \Delta H_D(\text{M(I)}) = & E(\text{Cs}_8\text{Ag}_{4-x}\text{M(I)}_x\text{Bi}_4\text{Cl}_{24}) - (4-x) E(\text{AgCl}) - 8E(\text{CsCl}) \\ & - 4E(\text{BiCl}_3) - xE(\text{M(I)Cl}) \end{aligned} \quad (1)$$

$$\begin{aligned} \Delta H_D(\text{M(II)}) &= E(\text{Cs}_8\text{Ag}_3\text{M(II)}_2\text{Bi}_3\text{Cl}_{24}) - 3E(\text{AgCl}) - 8E(\text{CsCl}) \\ &\quad - 3E(\text{BiCl}_3) - 2E(\text{M(II)Cl}_2) \end{aligned} \quad (2)$$

$$\begin{aligned} \Delta H_D(\text{M(III)}) &= E(\text{Cs}_8\text{Ag}_4\text{M(III)}_x\text{Bi}_{4-x}\text{Cl}_{24}) - 4E(\text{AgCl}) - 8E(\text{CsCl}) \\ &\quad - (4-x)E(\text{BiCl}_3) - xE(\text{M(III)Cl}_3) \end{aligned} \quad (3)$$

In Equation 1 and 3, x can have value 1, 2, 3 or 4. Based on the band gap and ΔH_D (calculated using PBE+SOC), a pre-screening process has been employed to find the suitable configurations. In Figure 6(a), the promising configurations lie within the shaded region for which band gap is varying from 0.0 to 1.5 eV (for further details see Table S2, S3 and S4 in SI). For all the prescreened configurations of double perovskite, ΔH_D is negative, indicating that all the considered systems are stable and these will not decompose into respective binary components. Subsequently, we have calculated ΔH_D and band gap using HSE06+SOC ϵ_{xc} functional for aforementioned selected configurations (see Figure 6(b)). In Figure 6(b), restoring Shockley-Queisser (SQ) criterion,³⁶ we have identified 19 double perovskite configurations for which band gap lies within 1.0 to 2.3 eV, which is relevant for solar cell and other optoelectronic devices.

Note that on increasing the concentration of the external element, if the band gap is increased (or decreased), it increases (or decreases) consistently on further increasing the concentration.³⁷ However, in some cases, we have noticed an irregular change in band gap on varying the concentration of the alloying atoms. For instance, on increasing the percentage of Sb at Bi-sites, band gap decreases up to 75% substitution, and thereafter, an increment in band gap has been observed on 100% substitution. Similar kind of change in band gap has also been observed on complete substitution of other elements at Ag or Bi site (see Table S2, S3 and S4 in SI for details). To understand this change in the band gap on 100% substitution of Sb, we have plotted the band structures of Sb-alloyed system with different concentrations of Sb (see Figure 5). We can clearly see that on 100% substitution of Sb at Bi-sites, the lowest energy level in the conduction band corresponding to Bi-orbitals (that is

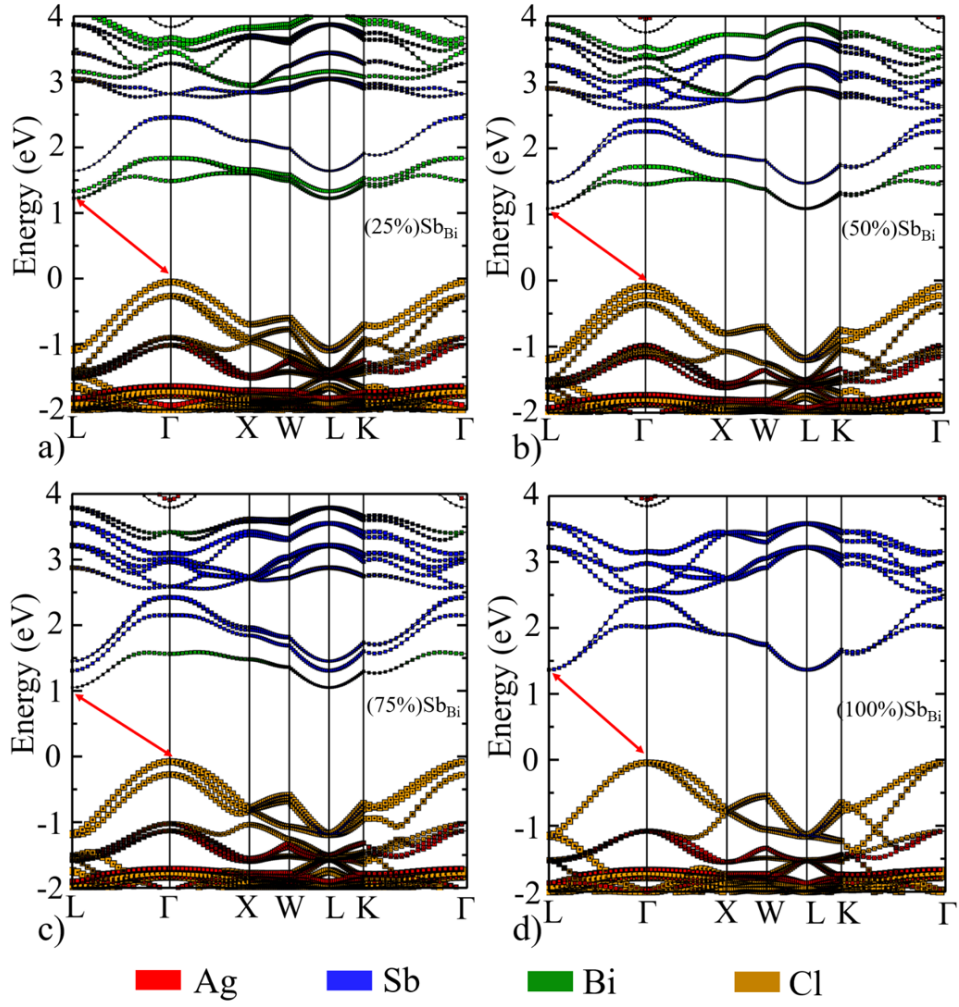


Figure 2: Band structure of (a) $\text{Cs}_8\text{Ag}_4\text{Sb}_1\text{Bi}_3\text{Cl}_{24}$, (b) $\text{Cs}_8\text{Ag}_4\text{Sb}_2\text{Bi}_2\text{Cl}_{24}$, (c) $\text{Cs}_8\text{Ag}_4\text{Sb}_3\text{Bi}_1\text{Cl}_{24}$ and (d) $\text{Cs}_8\text{Ag}_4\text{Sb}_4\text{Cl}_{24}$ using PBE+SOC ϵ_{xc} functional.

present in Figure 5(a-c)) disappears. Consequently, there is an increment in the band gap (see Figure 5(d)). In addition, from Figure 5, we can see that SOC effect is attributed to the fundamental mismatch of Ag- and Bi-orbitals, which is also mentioned by Savory et al.³⁸ Similar SOC effect can be observed from band structures for Au substitution at Ag-sites as well (see Figure S3 in SI). Hence, in some cases, on complete substitution either at Ag- or Bi-sites, there is an inconsistent change in the band gap (i.e., on complete substitution of Ag with Na, K etc., similar inconsistency has been observed). For more details also see Figure S4 and S5.

Next, we have determined the optical properties of the 19 potential candidate structures (viz. $\text{Cs}_8\text{Ag}_{4-x}\text{M(I)}_x\text{Bi}_4\text{Cl}_{24}$ ($\text{M(I)} = \text{Au}$ and Cu); $x \in [1, 4]$), $\text{Cs}_8\text{Ag}_3\text{M(II)}_2\text{Bi}_3\text{Cl}_{24}$ ($\text{M(II)} = \text{Sn, Ge, Rh, Ni, Co, Cd, Mn}$ and Zn), and $\text{Cs}_8\text{Ag}_4\text{Sb}_x\text{Bi}_{4-x}\text{Cl}_{24}$ ($x \in [1, 3]$), which possess band gap in an appropriate range for solar cell and other optoelectronic applications. To determine optical properties, frequency dependent complex dielectric function, $\varepsilon(\omega) = \text{Re}(\varepsilon) + \text{Im}(\varepsilon)$ has been calculated using HSE06+SOC ϵ_{xc} functional as shown in Figure 3 (the results of optical properties without SOC are shown in Figure S6 and S7 in SI for benchmark purpose). Therefore, using $\text{Re}(\varepsilon)$ and $\text{Im}(\varepsilon)$ of dielectric function, various optical properties, e.g., refractive index (η), extinction coefficient (κ), and absorption coefficient (α) can be computed using following expressions:

$$\eta = \frac{1}{\sqrt{2}} \left[\sqrt{\text{Re}(\varepsilon)^2 + \text{Im}(\varepsilon)^2} + \text{Re}(\varepsilon) \right]^{\frac{1}{2}} \quad (4)$$

$$\kappa = \frac{1}{\sqrt{2}} \left[\sqrt{\text{Re}(\varepsilon)^2 + \text{Im}(\varepsilon)^2} - \text{Re}(\varepsilon) \right]^{\frac{1}{2}} \quad (5)$$

$$\alpha = \frac{2\omega\kappa}{c} \quad (6)$$

Here, in Equation 6, ω and c correspond to angular frequency and speed of light, respectively. In Figure 3(a), peaks of conformers are red shifted w.r.t. $\text{Cs}_2\text{AgBiCl}_6$. Here, red shift is attributed to the reduction of the band gap. There is more red shift on increasing the concentration of Au in comparison to Cu. On the other hand, the real part of the dielectric

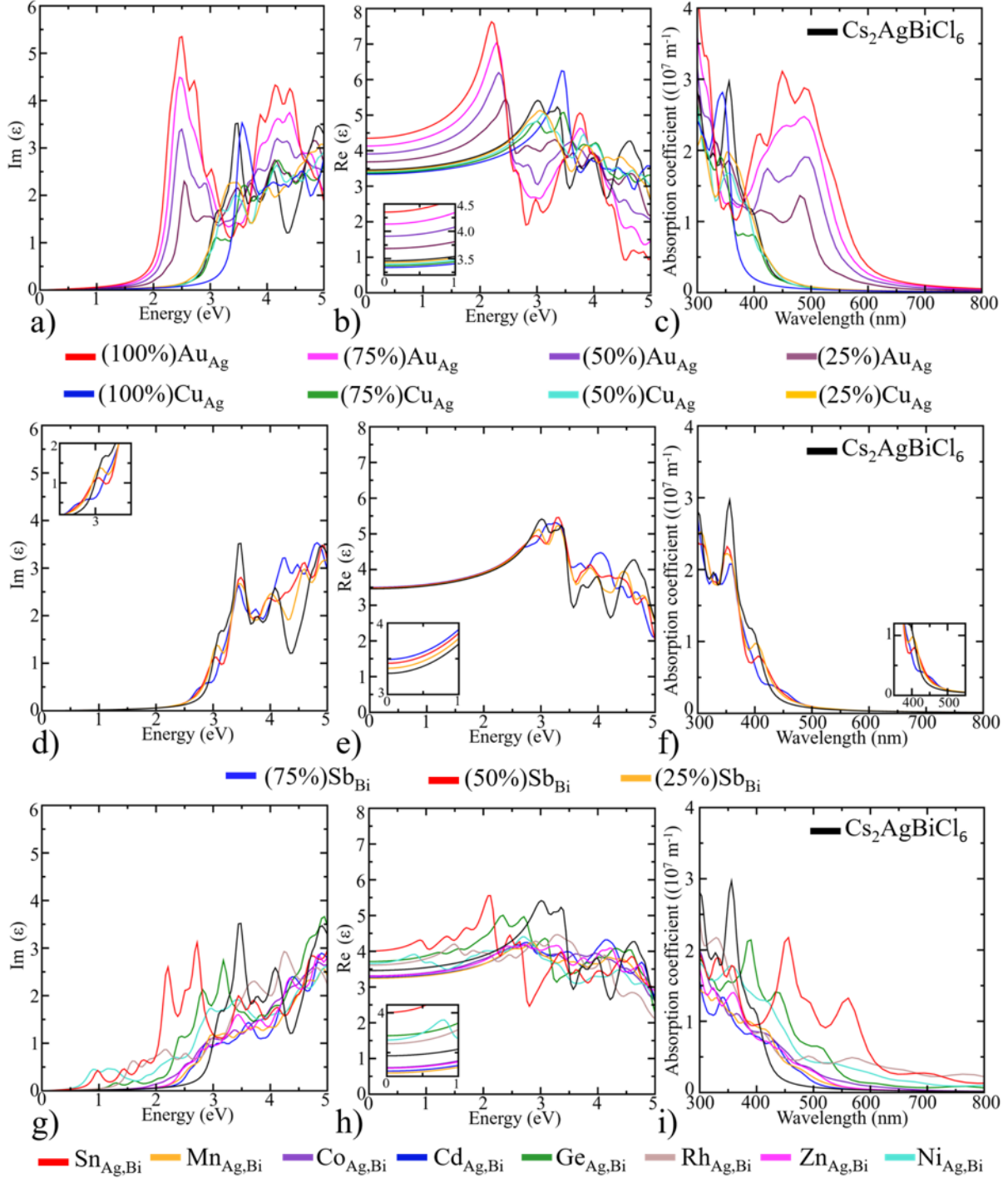


Figure 3: Variation of imaginary part of dielectric constant ($\text{Im}(\epsilon)$) of $\text{Cs}_2\text{AgBiCl}_6$ sublattice mixed with (a) monovalent (M(I)), (d) divalent (M(II)) and (g) trivalent (M(III)) cations, respectively. Variation of real part of dielectric constant ($\text{Re}(\epsilon)$) of $\text{Cs}_2\text{AgBiCl}_6$ sublattice mixed with (b) monovalent (M(I)), (e) divalent (M(II)) and (h) trivalent (M(III)) cations, respectively. Absorption coefficient of $\text{Cs}_2\text{AgBiCl}_6$ sublattice mixed with (c) monovalent (M(I)), (f) divalent (M(II)) and (i) trivalent (M(III)) cations, respectively. Note that all calculations have been done using HSE06+SOC ϵ_{xc} functional.

constant ($\omega = 0$) increases, with increase in the concentration of Au and decreases, with increase in the concentration of Cu (see Figure 3(b)). For high degree of charge screening, which can prohibit radiative electron-hole recombination, a large value of $\text{Re}(\omega)$ at $\omega = 0$ is indispensable.³⁹ Hence, the solar cell absorber, which exhibits large $\text{Re}(\omega)$ at $\omega = 0$ is more efficient. In view of this, Au substitution is more beneficial than Cu for replacing Ag-sites.

In Figure 3(c), we can clearly see that peaks corresponding to Au substitution are red shifted w.r.t. $\text{Cs}_2\text{AgBiCl}_6$ and show good optical absorption within visible region. Hence, we have discerned that in case of alloying with M(I), substitution of Au at Ag-sites acts as a promising candidate rather than Cu. Likewise, in case of alloying with M(III), substitution with Sb at Bi-sites acts as a promising candidate. From Figure 3(d), the red shift w.r.t. pristine (see inset to have a clear view) conveys that band gap decreases on increasing the concentration of Sb. However, for 100% Sb_{Bi} , band gap increases, which can be seen from band structure (see Figure 5(d)). From Figure 3(e) and 3(f), we can see that optical properties are enhanced on increasing the concentration of Sb (upto 75%) w.r.t. pristine. Similarly, in case of alloying with M(II), from Figure 3(g) and 3(i), there is a red shift of absorption peak w.r.t. $\text{Cs}_2\text{AgBiCl}_6$. Moreover, static value of $\text{Re}(\omega)$ at $\omega = 0$ for $\text{Sn}_{\text{Ag,Bi}}$, $\text{Rh}_{\text{Ag,Bi}}$, $\text{Ni}_{\text{Ag,Bi}}$ and $\text{Ge}_{\text{Ag,Bi}}$ is larger than pristine system; but for other alloyed systems (viz. $\text{Zn}_{\text{Ag,Bi}}$, $\text{Co}_{\text{Ag,Bi}}$, and $\text{Mn}_{\text{Ag,Bi}}$), it is lower than pristine system (see Figure 3(h)). Out of all the M(II) selected candidates, these four (viz. Sn, Rh, Ni and Ge) are the best aspirants. Although, only $\text{Sn}_{\text{Ag,Bi}}$ and $\text{Ge}_{\text{Ag,Bi}}$ show direct band gap, the other two are to be more suitable for optoelectronic devices excluding solar cell. On the other hand, since Sn is cheaper than Ge, it serves as better candidate for alloying. It has been reported that complete substitution of Sn degrades the properties of the system.^{14,15} Therefore, in order to overcome this problem, we have done partial substitution of Sn. Also, from Figure 3, we can compare the scales (viz. values of dielectric constants and peaks of absorption coefficient in visible region) and infer that alloying with M(II) is a better choice to enhance the optical properties. On comparing all the above results in Figure 6 and 3, we have

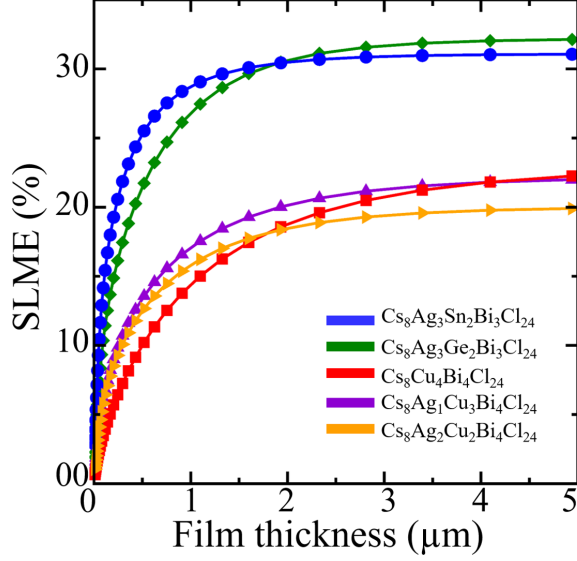


Figure 4: Variation of SLME w.r.t. the thickness of solar cell absorber.

revealed that partial Sn substitution acts as a promising candidate to enhance the optical properties of $\text{Cs}_2\text{AgBiCl}_6$ without degrading the stability. In addition, it also exhibits direct band gap property (see Figure S4 in SI). Thus $\text{Sn}_{\text{Ag,Bi}}$ acts as a rational candidate for solar cell application.

Lastly, to design highly efficient solar cell absorber, spectroscopic limited maximum efficiency (SLME)³⁴ has been calculated. The SLME is based on the improved Shockley-Queisser model. It depends on the absorption coefficient, thickness of the film absorber and nature of the band gap of the material. For an efficient solar cell, Yu et al.⁴⁰ have proposed the concept of SLME based on Fermi Golden rule. According to Fermi Golden rule, the optical absorption is directly proportional to

$$\frac{2\pi}{\hbar} \int |\langle \nu | \hat{H} | c \rangle|^2 \frac{2}{8\pi^3} \delta(E_c(\vec{k}) - E_\nu(\vec{k}) - \hbar\omega) d^3k \quad (7)$$

where $\langle \nu | \hat{H} | c \rangle$ is the transition matrix. $\hbar\omega$ is the photonic energy required for transition from states in valence band (ν) to the states in conduction band (c). In Equation 7, integration goes over the whole reciprocal space. We have calculated the SLME of those alloyed

systems, which possess direct band gap, as a function of thickness of the absorber layer (see Figure 7). Here, in Table 3, we have shown SLME of few double perovskites at 5 μm and compared our results with other efficient hybrid perovskites that are reported recently. From

Table 1: Comparison of SLME of double perovskites with hybrid perovskite at 5 μm absorber layer thickness.

Conformers	SLME (%)
$\text{Cs}_8\text{Ag}_3\text{Ge}_2\text{Bi}_3\text{Cl}_{24}$	32.08
$\text{Cs}_8\text{Ag}_3\text{Sn}_2\text{Bi}_3\text{Cl}_{24}$	30.91
$\text{Cs}_8\text{Cu}_4\text{Bi}_4\text{Cl}_{24}$	22.24
$\text{Cs}_8\text{Ag}_1\text{Cu}_3\text{Bi}_4\text{Cl}_{24}$	21.85
$\text{Cs}_8\text{Ag}_2\text{Cu}_2\text{Bi}_4\text{Cl}_{24}$	19.80
$\text{MA}_8\text{Pb}_8\text{I}_{24}$	31.02 ⁶
$\text{MA}_8\text{Pb}_7\text{Sn}_1\text{I}_{24}$	33.02 ⁶
$\text{FA}_8\text{Pb}_4\text{Sn}_4\text{Br}_{24}$	26.74 ⁴¹

Table 3, SLME of $\text{Cs}_8\text{Ag}_3\text{Ge}_2\text{Bi}_3\text{Cl}_{24}$ and $\text{Cs}_8\text{Ag}_3\text{Sn}_2\text{Bi}_3\text{Cl}_{24}$ are 32.08% and 30.91%, respectively. These numbers are very much encouraging from application perspective in solar cells. In addition, they are more stable, while in contact with air and moisture as compared to IO hybrid perovskites.^{31,42}

In summary, we have presented a thorough study of alloying double perovskite $\text{Cs}_2\text{AgBiCl}_6$ with M(I), M(II) and M(III) cations. The role of SOC is important to accurately predict the band gap and band-edge positions in such systems. All the mixed sublattices are structurally stable as indicated by the Goldschmidt’s tolerance factor and octahedral factor. The enthalpies of decomposition are negative, indicating the thermodynamic stability of alloyed systems. We have revealed that for substitution at Bi-sites, on increasing the concentration of Sb, band gap decreases upto 75% Sb_{Bi} substitution. However, there is a sudden increase in band gap for 100% Sb_{Bi} due to complete removal of Bi. We have also identified that Au substitution can enhance the optical properties effectively due to reduction in band gap. Hence, we have concluded that partial substitution of Au and Sb at Ag- and Bi-sites, respectively, will be cost-effective and efficient to enhance the optical properties. Out of alloying with

M(I), M(II) and M(III), M(II) ($\text{Sn}_{\text{Ag,Bi}}$, $\text{Rh}_{\text{Ag,Bi}}$, $\text{Ni}_{\text{Ag,Bi}}$ and $\text{Ge}_{\text{Ag,Bi}}$) substitutions come out to be superior for optical properties. However, only in case of $\text{Sn}_{\text{Ag,Bi}}$ and $\text{Ge}_{\text{Ag,Bi}}$, direct band gaps are noticed. SLME of $\text{Cs}_8\text{Ag}_3\text{Ge}_2\text{Bi}_3\text{Cl}_{24}$ and $\text{Cs}_8\text{Ag}_3\text{Sn}_2\text{Bi}_3\text{Cl}_{24}$ are 32.08% and 30.91%, respectively, which definitely suggest huge promise towards prospective solar cell absorbers.

Computational Methods

First-principles calculations have been performed using DFT with PAW pseudopotential method^{43–45} as implemented in Vienna *ab initio* simulation package (VASP).⁴⁶ $\text{Cs}_2\text{AgBiCl}_6$ is a cubic structure having space group *Pnma*. It comprises of 40 atoms (4 formula units) in the unit cell i.e., $\text{Cs}_8\text{Ag}_4\text{Bi}_4\text{Cl}_{24}$ and single defect state remains fully localized with periodic boundary conditions. We have used exchange-correlation (ϵ_{xc}) functionals viz. GGA (PBE²⁹) and hybrid functional HSE06³⁰ with and without SOC for the calculations. The total energy tolerance is set to 0.001 meV. The Hellmann-Feynman forces⁴⁷ have been converged upto 0.001 eV/Å by conjugate gradient (CG) minimization to obtain optimized ground state structures. The k-mesh has been generated by the Monkhorst-Pack⁴⁸ method. All the structures are fully relaxed with k-mesh $2 \times 2 \times 2$. For single-point energy calculation, k-mesh is converged and kept fixed at $5 \times 5 \times 5$. The plane wave energy cut-off is set to 600 eV in our calculations.

Acknowledgement

DG acknowledges UGC, India, for the junior research fellowship [grant no.: 1268/(CSIR-UGC NET JUNE 2018)]. PB acknowledges UGC, India, for the junior research fellowship [grant no.: 1392/(CSIR-UGC NET JUNE 2018)]. MK acknowledges CSIR, India, for the senior research fellowship [grant no.: 09/086(1292)/2017-EMR-I]. SB acknowledges the financial support from SERB under core research grant (grant no. CRG/2019/000647). We

acknowledge the High Performance Computing (HPC) facility at IIT Delhi for computational resources.

Supporting Information Available

The following files are available free of charge. Details regarding band gap using different functionals for various conformers, optical properties using HSE06, and partial density of states (pDOS) have been given in the supporting information file.

Supplemental Material

- I.** Band gap, tolerance factor, octahedral factor and enthalpy of decomposition of different configurations
- II.** Band structures for Au and Sn substitution
- III.** Partial density of states (pDOS) plot, showing contribution of various orbitals in valence band maximum (VBM) and conduction band minimum (CBm) of few selected conformers
- IV.** Optical properties using HSE06 ϵ_{xc} functional

Band gap, tolerance factor, octahedral factor and enthalpy of decomposition of different configurations

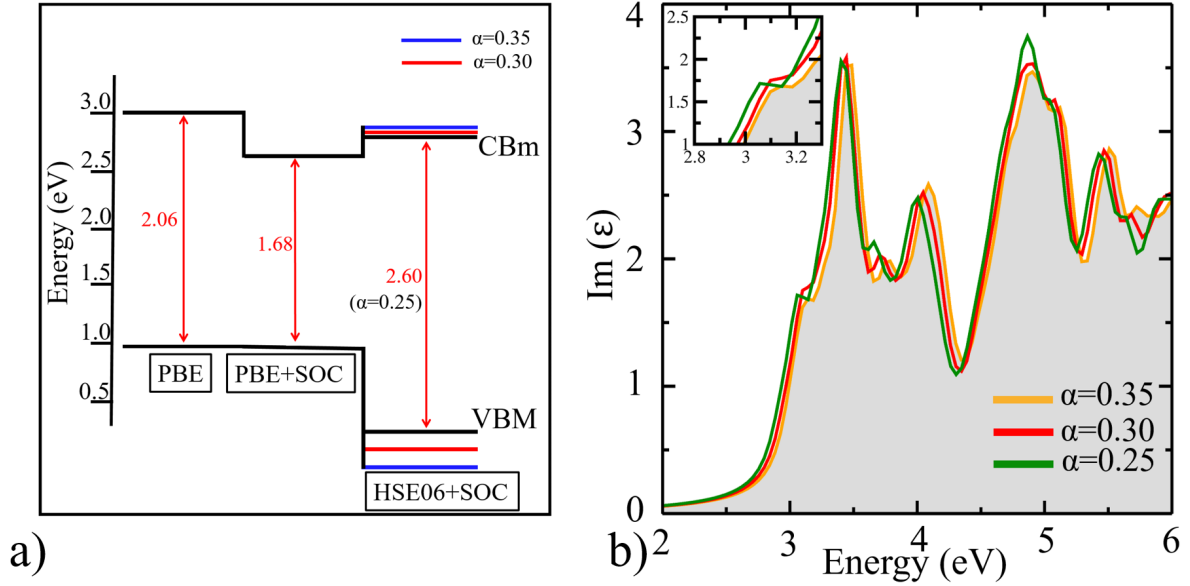


Figure 5: (a) Band edge alignment of VBM and CBm with PBE, PBE+SOC and HSE06+SOC and (b) Absorption spectra of $\text{Cs}_2\text{AgBiCl}_6$ using HSE06+SOC ϵ_{xc} functional, where band gaps of 2.60, 2.79 and 2.99 eV have been obtained with Hartree-Fock exchange fraction (α) = 0.25, 0.30 and 0.35, respectively.

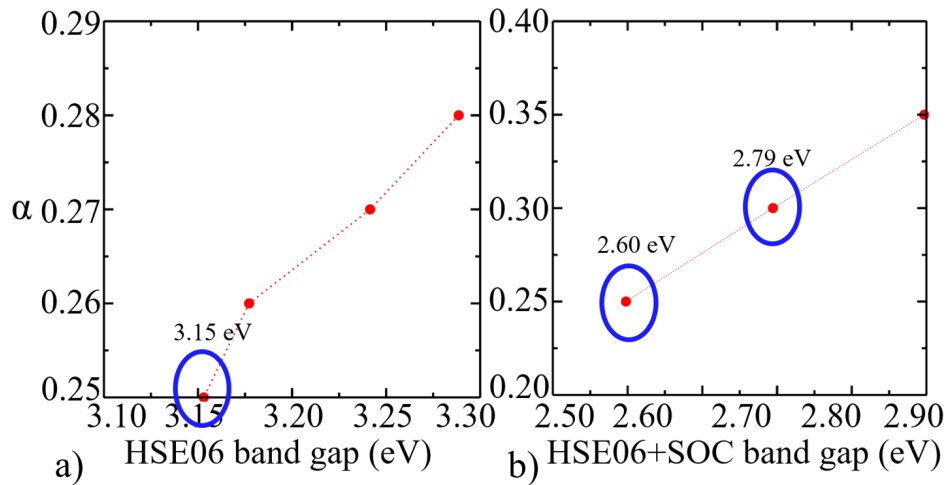


Figure 6: Band gap of $\text{Cs}_2\text{AgBiCl}_6$, using HSE06 and HSE06+SOC ϵ_{xc} functionals with different values of Hartree-Fock exchange fraction (α).

In Figure 5(a), shifting of band edges viz. conduction band minimum (CBm) and valence band maximum (VBM) positions on implementation of different ϵ_{xc} functionals viz. PBE, PBE+SOC and HSE06+SOC have been shown. Correct positions of band edges are mandatory for prediction of excited state properties of a material. An estimated band gap of $\text{Cs}_2\text{AgBiCl}_6$ with PBE is 2.06 eV, which is not in agreement with experimental value of 2.77 eV. Next, spin-orbit coupling (SOC) effect has been incorporated. It lowers the CBm owing to splitting of degenerate levels, without altering the VBM. Hence, PBE+SOC gives reduced band gap value (see Figure 5(a)). Apart from this, the presence of self-interaction error in PBE leads to an incorrect position of VBM. Partial elimination of self-interaction error can be achieved on incorporating hybrid ϵ_{xc} functional that takes into account Hartree-Fock exchange fraction (α). With different values of α i.e. 0.25, 0.30 and 0.35, the obtained band gaps are 2.60 eV, 2.79 eV and 2.99 eV, respectively (see Figure 5(b)). The band gap diverges from the experimental value on increasing α beyond 0.30. The default value of α i.e., 0.25 also gives band gap in good approximation with the experimental value. In Figure 5(b), the imaginary part of the dielectric function corresponding to three different values of $\alpha = 0.25, 0.30$ and 0.35 has been calculated. From the positions of three peaks, it is confirmed that on increasing the value of α , band gap increases.

Table 2: Tolerance and octahedral factor of different conformers

Conformers	Tolerance factor (t)	Octahedral factor (μ)
$\text{Cs}_8\text{Ag}_4\text{Bi}_4\text{Cl}_{24}$	0.90	0.60
$\text{Cs}_8\text{Ag}_3\text{Au}_1\text{Bi}_4\text{Cl}_{24}$	0.89	0.62
$\text{Cs}_8\text{Ag}_2\text{Au}_2\text{Bi}_4\text{Cl}_{24}$	0.88	0.63
$\text{Cs}_8\text{Ag}_1\text{Au}_3\text{Bi}_4\text{Cl}_{24}$	0.87	0.65
$\text{Cs}_8\text{Au}_4\text{Bi}_4\text{Cl}_{24}$	0.87	0.66
$\text{Cs}_8\text{Ag}_3\text{Cu}_1\text{Bi}_4\text{Cl}_{24}$	0.91	0.58

$\text{Cs}_8\text{Ag}_2\text{Cu}_2\text{Bi}_4\text{Cl}_{24}$	0.93	0.55
$\text{Cs}_8\text{Ag}_1\text{Cu}_3\text{Bi}_4\text{Cl}_{24}$	0.95	0.52
$\text{Cs}_8\text{Cu}_4\text{Bi}_4\text{Cl}_{24}$	0.96	0.50
$\text{Cs}_8\text{Ag}_3\text{In}_1\text{Bi}_4\text{Cl}_{24}$	0.91	0.58
$\text{Cs}_8\text{Ag}_2\text{In}_2\text{Bi}_4\text{Cl}_{24}$	0.93	0.55
$\text{Cs}_8\text{Ag}_1\text{In}_3\text{Bi}_4\text{Cl}_{24}$	0.94	0.53
$\text{Cs}_8\text{In}_4\text{Bi}_4\text{Cl}_{24}$	0.96	0.51
$\text{Cs}_8\text{Ag}_3\text{K}_1\text{Bi}_4\text{Cl}_{24}$	0.89	0.62
$\text{Cs}_8\text{Ag}_2\text{K}_2\text{Bi}_4\text{Cl}_{24}$	0.88	0.63
$\text{Cs}_8\text{Ag}_1\text{K}_3\text{Bi}_4\text{Cl}_{24}$	0.87	0.65
$\text{Cs}_8\text{K}_4\text{Bi}_4\text{Cl}_{24}$	0.87	0.66
$\text{Cs}_8\text{Ag}_3\text{Na}_1\text{Bi}_4\text{Cl}_{24}$	0.90	0.59
$\text{Cs}_8\text{Ag}_2\text{Na}_2\text{Bi}_4\text{Cl}_{24}$	0.91	0.58
$\text{Cs}_8\text{Ag}_1\text{Na}_3\text{Bi}_4\text{Cl}_{24}$	0.92	0.58
$\text{Cs}_8\text{Na}_4\text{Bi}_4\text{Cl}_{24}$	0.92	0.57
$\text{Cs}_8\text{Ag}_3\text{Ti}_1\text{Bi}_4\text{Cl}_{24}$	0.91	0.58
$\text{Cs}_8\text{Ag}_2\text{Ti}_2\text{Bi}_4\text{Cl}_{24}$	0.92	0.56
$\text{Cs}_8\text{Ag}_1\text{Ti}_3\text{Bi}_4\text{Cl}_{24}$	0.93	0.54
$\text{Cs}_8\text{Ti}_4\text{Bi}_4\text{Cl}_{24}$	0.95	0.52
$\text{Cs}_8\text{Ag}_4\text{Cr}_1\text{Bi}_3\text{Cl}_{24}$	0.91	0.59
$\text{Cs}_8\text{Ag}_4\text{Cr}_2\text{Bi}_2\text{Cl}_{24}$	0.92	0.57
$\text{Cs}_8\text{Ag}_4\text{Cr}_3\text{Bi}_1\text{Cl}_{24}$	0.93	0.55
$\text{Cs}_8\text{Ag}_4\text{Cr}_4\text{Cl}_{24}$	0.94	0.54
$\text{Cs}_8\text{Ag}_4\text{Ga}_1\text{Bi}_3\text{Cl}_{24}$	0.92	0.57
$\text{Cs}_8\text{Ag}_4\text{Ga}_2\text{Bi}_2\text{Cl}_{24}$	0.93	0.55
$\text{Cs}_8\text{Ag}_4\text{Ga}_3\text{Bi}_1\text{Cl}_{24}$	0.95	0.52

$\text{Cs}_8\text{Ag}_4\text{Ga}_4\text{Cl}_{24}$	0.97	0.49
$\text{Cs}_8\text{Ag}_4\text{In}_1\text{Bi}_3\text{Cl}_{24}$	0.91	0.59
$\text{Cs}_8\text{Ag}_4\text{In}_2\text{Bi}_2\text{Cl}_{24}$	0.92	0.57
$\text{Cs}_8\text{Ag}_4\text{In}_3\text{Bi}_1\text{Cl}_{24}$	0.93	0.55
$\text{Cs}_8\text{Ag}_4\text{In}_4\text{Cl}_{24}$	0.94	0.54
$\text{Cs}_8\text{Ag}_4\text{Sb}_1\text{Bi}_3\text{Cl}_{24}$	0.91	0.58
$\text{Cs}_8\text{Ag}_4\text{Sb}_2\text{Bi}_2\text{Cl}_{24}$	0.92	0.56
$\text{Cs}_8\text{Ag}_4\text{Sb}_3\text{Bi}_1\text{Cl}_{24}$	0.93	0.55
$\text{Cs}_8\text{Ag}_4\text{Sb}_4\text{Cl}_{24}$	0.94	0.53
$\text{Cs}_8\text{Ag}_4\text{Sc}_1\text{Bi}_3\text{Cl}_{24}$	0.91	0.58
$\text{Cs}_8\text{Ag}_4\text{Sc}_2\text{Bi}_2\text{Cl}_{24}$	0.92	0.56
$\text{Cs}_8\text{Ag}_4\text{Sc}_3\text{Bi}_1\text{Cl}_{24}$	0.93	0.54
$\text{Cs}_8\text{Ag}_4\text{Sc}_4\text{Cl}_{24}$	0.95	0.52
$\text{Cs}_8\text{Ag}_4\text{Tl}_1\text{Bi}_3\text{Cl}_{24}$	0.91	0.60
$\text{Cs}_8\text{Ag}_4\text{Tl}_2\text{Bi}_2\text{Cl}_{24}$	0.91	0.58
$\text{Cs}_8\text{Ag}_4\text{Tl}_3\text{Bi}_1\text{Cl}_{24}$	0.92	0.57
$\text{Cs}_8\text{Ag}_4\text{Tl}_4\text{Cl}_{24}$	0.92	0.56
$\text{Cs}_8\text{Ag}_4\text{Y}_1\text{Bi}_3\text{Cl}_{24}$	0.90	0.59
$\text{Cs}_8\text{Ag}_4\text{Y}_2\text{Bi}_2\text{Cl}_{24}$	0.91	0.58
$\text{Cs}_8\text{Ag}_4\text{Y}_3\text{Bi}_1\text{Cl}_{24}$	0.92	0.58
$\text{Cs}_8\text{Ag}_4\text{Y}_4\text{Cl}_{24}$	0.92	0.57
$\text{Cs}_8\text{Ag}_3\text{Cd}_2\text{Bi}_3\text{Cl}_{24}$	0.91	0.58
$\text{Cs}_8\text{Ag}_3\text{Co}_2\text{Bi}_3\text{Cl}_{24}$	0.93	0.55
$\text{Cs}_8\text{Ag}_3\text{Cu}_2\text{Bi}_3\text{Cl}_{24}$	0.93	0.55
$\text{Cs}_8\text{Ag}_3\text{Ge}_2\text{Bi}_3\text{Cl}_{24}$	0.93	0.55
$\text{Cs}_8\text{Ag}_3\text{Mn}_2\text{Bi}_3\text{Cl}_{24}$	0.93	0.54

$\text{Cs}_8\text{Ag}_3\text{Ni}_2\text{Bi}_3\text{Cl}_{24}$	0.94	0.54
$\text{Cs}_8\text{Ag}_3\text{Sn}_2\text{Bi}_3\text{Cl}_{24}$	0.90	0.61
$\text{Cs}_8\text{Ag}_3\text{V}_2\text{Bi}_3\text{Cl}_{24}$	0.92	0.56
$\text{Cs}_8\text{Ag}_3\text{Zn}_2\text{Bi}_3\text{Cl}_{24}$	0.93	0.55
$\text{Cs}_8\text{Ag}_3\text{Rh}_2\text{Bi}_3\text{Cl}_{24}$	0.93	0.55

Table 3: Band gap and enthalpy of decomposition of different conformers (double perovskites) for M(III) substitution

Conformers	PBE (eV)	PBE +SOC (eV)	HSE06 +SOC (eV)	HSE06 (eV)	ΔH_D (PBE+SOC) (eV)	ΔH_D (HSE06+SOC) (eV)
$\text{Cs}_8\text{Ag}_4\text{Cr}_1\text{Bi}_3\text{Cl}_{24}$	1.47	1.34	2.37	-	-9.19	-11.25
$\text{Cs}_8\text{Ag}_4\text{Cr}_2\text{Bi}_2\text{Cl}_{24}$	1.10	1.03	2.06	2.43	-8.96	-11.77
$\text{Cs}_8\text{Ag}_4\text{Cr}_3\text{Bi}_1\text{Cl}_{24}$	0.78	0.77	2.73	2.86	-8.65	-12.29
$\text{Cs}_8\text{Ag}_4\text{Cr}_4\text{Cl}_{24}$	0.80	0.79	2.81	2.94	-8.27	-12.81
$\text{Cs}_8\text{Ag}_4\text{Ga}_1\text{Bi}_3\text{Cl}_{24}$	1.91	1.55	2.52	-	-9.20	-10.84
$\text{Cs}_8\text{Ag}_4\text{Ga}_2\text{Bi}_2\text{Cl}_{24}$	1.57	1.38	2.45	-	-8.98	-
$\text{Cs}_8\text{Ag}_4\text{Ga}_3\text{Bi}_1\text{Cl}_{24}$	2.17	2.03	3.11	-	-8.71	-10.17
$\text{Cs}_8\text{Ag}_4\text{Ga}_4\text{Cl}_{24}$	1.31	1.27	2.62	-	-8.33	-9.70
$\text{Cs}_8\text{Ag}_4\text{In}_1\text{Bi}_3\text{Cl}_{24}$	1.91	1.61	2.58	-	-9.43	-
$\text{Cs}_8\text{Ag}_4\text{In}_2\text{Bi}_2\text{Cl}_{24}$	1.52	1.37	2.40	-	-9.47	-11.30
$\text{Cs}_8\text{Ag}_4\text{In}_3\text{Bi}_1\text{Cl}_{24}$	2.04	1.97	3.07	-	-9.16	-
$\text{Cs}_8\text{Ag}_4\text{In}_4\text{Cl}_{24}$	1.19	1.17	2.56	-	-9.46	-11.38
$\text{Cs}_8\text{Ag}_4\text{Sb}_1\text{Bi}_3\text{Cl}_{24}$	1.80	1.44	2.31	-	-9.30	-10.94
$\text{Cs}_8\text{Ag}_4\text{Sb}_2\text{Bi}_2\text{Cl}_{24}$	1.71	1.37	2.22	-	-9.23	-10.76
$\text{Cs}_8\text{Ag}_4\text{Sb}_3\text{Bi}_1\text{Cl}_{24}$	1.68	1.34	2.20	-	-9.16	-10.59
$\text{Cs}_8\text{Ag}_4\text{Sb}_4\text{Cl}_{24}$	1.69	1.64	2.57	-	-9.09	-
$\text{Cs}_8\text{Ag}_4\text{Sc}_1\text{Bi}_3\text{Cl}_{24}$	2.13	1.70	-	-	-9.27	-
$\text{Cs}_8\text{Ag}_4\text{Sc}_2\text{Bi}_2\text{Cl}_{24}$	2.18	1.69	-	-	-9.15	-
$\text{Cs}_8\text{Ag}_4\text{Sc}_3\text{Bi}_1\text{Cl}_{24}$	2.71	2.14	-	-	-9.01	-
$\text{Cs}_8\text{Ag}_4\text{Sc}_4\text{Cl}_{24}$	3.32	3.29	-	-	-8.84	-
$\text{Cs}_8\text{Ag}_4\text{Tl}_1\text{Bi}_3\text{Cl}_{24}$	0.65	0.62	-	-	-	-
$\text{Cs}_8\text{Ag}_4\text{Tl}_2\text{Bi}_2\text{Cl}_{24}$	0.45	0.42	-	-	-	-
$\text{Cs}_8\text{Ag}_4\text{Tl}_3\text{Bi}_1\text{Cl}_{24}$	0.83	0.82	0.45	0.42	-	-
$\text{Cs}_8\text{Ag}_4\text{Tl}_4\text{Cl}_{24}$	0.40	0.39	-	-	-	-
$\text{Cs}_8\text{Ag}_4\text{Y}_1\text{Bi}_3\text{Cl}_{24}$	2.11	1.74	-	-	-9.28	-
$\text{Cs}_8\text{Ag}_4\text{Y}_2\text{Bi}_2\text{Cl}_{24}$	2.28	1.80	-	-	-9.19	-
$\text{Cs}_8\text{Ag}_4\text{Y}_3\text{Bi}_1\text{Cl}_{24}$	2.87	2.21	-	-	-9.11	-
$\text{Cs}_8\text{Ag}_4\text{Y}_4\text{Cl}_{24}$	3.73	3.69	-	-	-9.01	-

Table 4: Band gap and enthalpy of decomposition of different conformers (double perovskites) for M(I) substitution

Conformers	PBE (eV)	PBE +SOC (eV)	HSE06 +SOC (eV)	HSE06 (eV)	ΔH_D (PBE+SOC) (eV)	ΔH_D (HSE06+SOC) (eV)
$\text{Cs}_8\text{Ag}_4\text{Bi}_4\text{Cl}_{24}$	2.06	1.67	2.60	3.15	-9.36	-11.11
$\text{Cs}_8\text{Ag}_3\text{Au}_1\text{Bi}_4\text{Cl}_{24}$	1.15	0.88	1.79	2.17	-9.18	-10.90
$\text{Cs}_8\text{Ag}_2\text{Au}_2\text{Bi}_4\text{Cl}_{24}$	1.02	0.76	1.62	2.01	-9.00	-10.70
$\text{Cs}_8\text{Ag}_1\text{Au}_3\text{Bi}_4\text{Cl}_{24}$	0.96	0.69	1.54	1.94	-8.80	-10.49
$\text{Cs}_8\text{Au}_4\text{Bi}_4\text{Cl}_{24}$	1.46	0.70	1.54	1.95	-8.62	-10.28
$\text{Cs}_8\text{Ag}_3\text{Cu}_1\text{Bi}_4\text{Cl}_{24}$	1.27	1.07	2.23	2.61	-9.26	-10.97
$\text{Cs}_8\text{Ag}_2\text{Cu}_2\text{Bi}_4\text{Cl}_{24}$	1.20	1.00	2.12	2.54	-9.15	-10.83
$\text{Cs}_8\text{Ag}_1\text{Cu}_3\text{Bi}_4\text{Cl}_{24}$	1.15	0.94	2.01	2.49	-9.04	-10.69
$\text{Cs}_8\text{Cu}_4\text{Bi}_4\text{Cl}_{24}$	1.13	0.89	1.95	2.48	-8.92	-10.54
$\text{Cs}_8\text{Ag}_3\text{In}_1\text{Bi}_4\text{Cl}_{24}$	0.45	0.07	0.39	1.22	-9.25	-11.01
$\text{Cs}_8\text{Ag}_2\text{In}_2\text{Bi}_4\text{Cl}_{24}$	0.30	0.13	0.11	1.10	-9.14	-10.90
$\text{Cs}_8\text{Ag}_1\text{In}_3\text{Bi}_4\text{Cl}_{24}$	0.14	0.23	0.17	0.98	-9.02	-10.80
$\text{Cs}_8\text{In}_4\text{Bi}_4\text{Cl}_{24}$	0.29	0.55	0.46	-	-8.89	-10.71
$\text{Cs}_8\text{Ag}_3\text{K}_1\text{Bi}_4\text{Cl}_{24}$	2.07	1.71	-	-	-10.37	-
$\text{Cs}_8\text{Ag}_2\text{K}_2\text{Bi}_4\text{Cl}_{24}$	2.15	1.80	-	-	-10.37	-
$\text{Cs}_8\text{Ag}_1\text{K}_3\text{Bi}_4\text{Cl}_{24}$	2.32	1.97	-	-	-10.86	-
$\text{Cs}_8\text{K}_4\text{Bi}_4\text{Cl}_{24}$	4.18	3.31	-	-	-11.34	-
$\text{Cs}_8\text{Ag}_3\text{Na}_1\text{Bi}_4\text{Cl}_{24}$	2.06	1.69	-	-	-9.36	-
$\text{Cs}_8\text{Ag}_2\text{Na}_2\text{Bi}_4\text{Cl}_{24}$	2.16	1.78	-	-	-9.36	-
$\text{Cs}_8\text{Ag}_1\text{Na}_3\text{Bi}_4\text{Cl}_{24}$	2.35	1.96	-	-	-9.36	-
$\text{Cs}_8\text{Na}_4\text{Bi}_4\text{Cl}_{24}$	3.12	3.09	-	-	-9.35	-
$\text{Cs}_8\text{Ag}_3\text{Ti}_1\text{Bi}_4\text{Cl}_{24}$	0.20	0.02	0.05	0.40	-9.10	-11.04
$\text{Cs}_8\text{Ag}_2\text{Ti}_2\text{Bi}_4\text{Cl}_{24}$	0.03	0.01	-	-	-8.88	-11.57
$\text{Cs}_8\text{Ag}_1\text{Ti}_3\text{Bi}_4\text{Cl}_{24}$	0.05	0.01	0.06	-	-8.71	-11.91
$\text{Cs}_8\text{Ti}_4\text{Bi}_4\text{Cl}_{24}$	0.04	0.01	0.02	-	-8.56	-12.51

Table 5: Band gap and enthalpy of decomposition of different conformers (double perovskites) for M(II) substitution

Conformers	PBE (eV)	PBE +SOC (eV)	HSE06 +SOC (eV)	HSE06 (eV)	ΔH_D (PBE+SOC) (eV)	ΔH_D (HSE06+SOC) (eV)
$\text{Cs}_8\text{Ag}_3\text{Cd}_2\text{Bi}_3\text{Cl}_{24}$	1.12	1.08	1.96	2.14	-9.12	-10.76
$\text{Cs}_8\text{Ag}_3\text{Co}_2\text{Bi}_3\text{Cl}_{24}$	0.77	0.71	2.01	-	-8.24	-11.79
$\text{Cs}_8\text{Ag}_3\text{Cu}_2\text{Bi}_3\text{Cl}_{24}$	Metal	Metal	-	-	-8.87	-
$\text{Cs}_8\text{Ag}_3\text{Ge}_2\text{Bi}_3\text{Cl}_{24}$	1.06	0.56	1.27	2.12	-9.18	-11.50
$\text{Cs}_8\text{Ag}_3\text{Mn}_2\text{Bi}_3\text{Cl}_{24}$	1.00	0.77	2.02	2.31	-9.56	-13.20
$\text{Cs}_8\text{Ag}_3\text{Mo}_2\text{Bi}_3\text{Cl}_{24}$	Metal	Metal	-	-	-8.31	-
$\text{Cs}_8\text{Ag}_3\text{Ni}_2\text{Bi}_3\text{Cl}_{24}$	0.79	0.07	1.64	1.73	-8.70	-11.63
$\text{Cs}_8\text{Ag}_3\text{Sn}_2\text{Bi}_3\text{Cl}_{24}$	1.05	0.41	1.06	2.07	-9.17	-10.87
$\text{Cs}_8\text{Ag}_3\text{V}_2\text{Bi}_3\text{Cl}_{24}$	1.90	0.31	0.77	1.26	-8.87	-11.74
$\text{Cs}_8\text{Ag}_3\text{Zn}_2\text{Bi}_3\text{Cl}_{24}$	1.04	0.93	1.87	2.05	-8.80	-10.43
$\text{Cs}_8\text{Ag}_3\text{Rh}_2\text{Bi}_3\text{Cl}_{24}$	0.50	0.19	1.32	1.76	-9.38	-11.99

Band structures for Au and Sn substitution

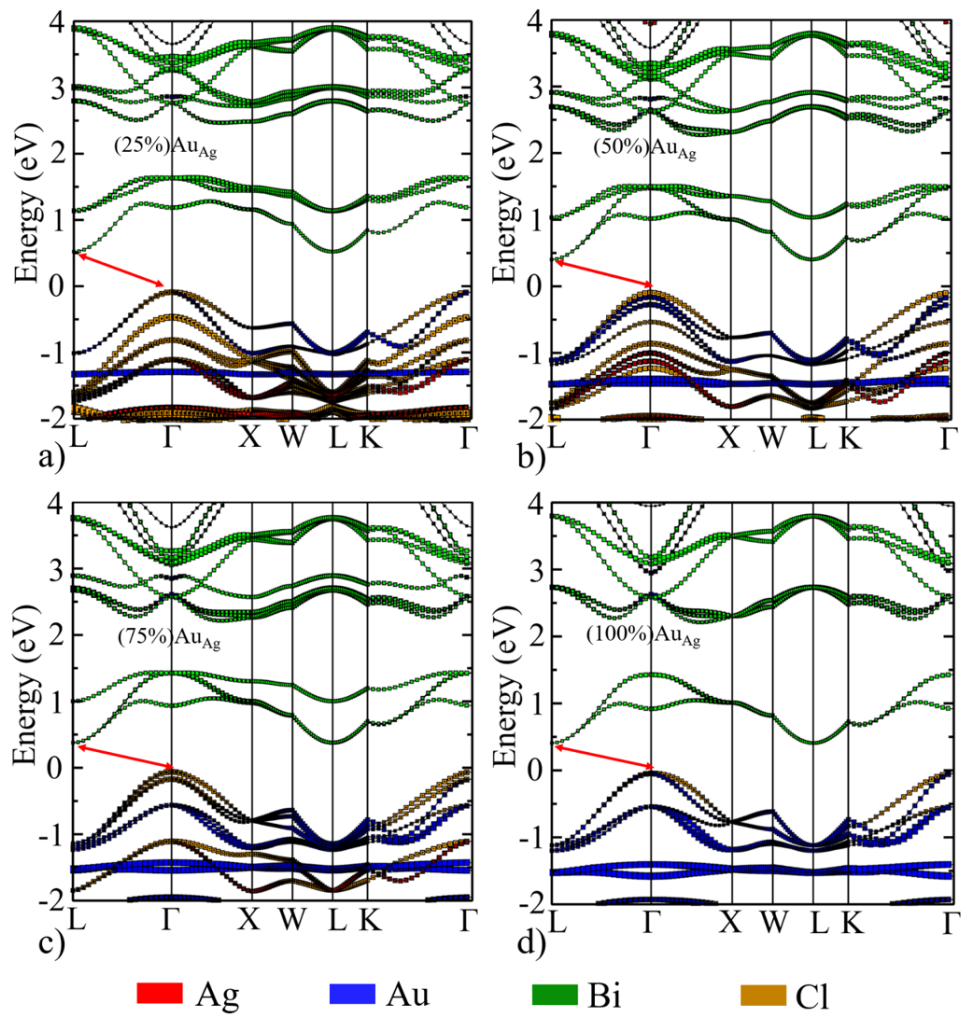


Figure 7: Band structure of (a) $\text{Cs}_8\text{Ag}_3\text{Au}_1\text{Bi}_4\text{Cl}_{24}$, (b) $\text{Cs}_8\text{Ag}_2\text{Au}_2\text{Bi}_4\text{Cl}_{24}$, (c) $\text{Cs}_8\text{Ag}_1\text{Au}_3\text{Bi}_4\text{Cl}_{24}$ and (d) $\text{Cs}_8\text{Au}_4\text{Bi}_4\text{Cl}_{24}$, using PBE+SOC ϵ_{xc} functional.

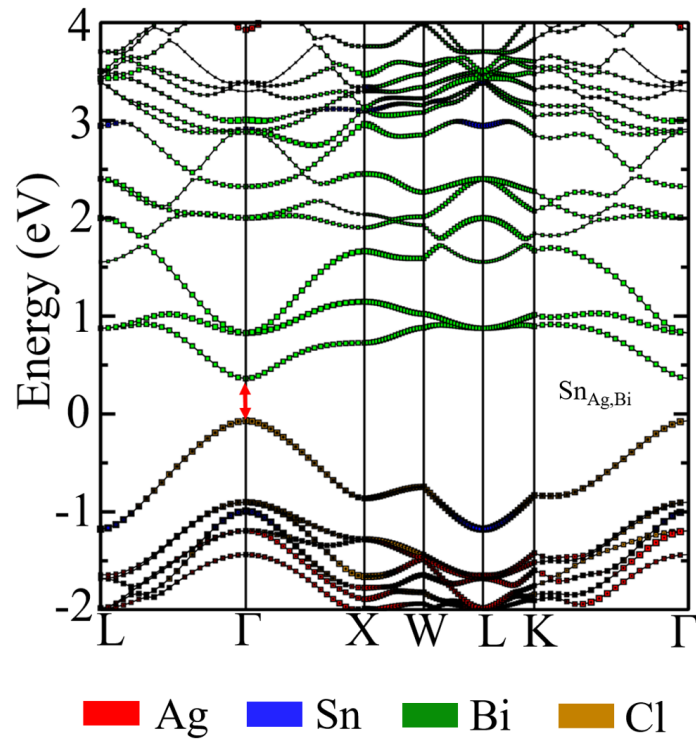


Figure 8: Band structure of $\text{Cs}_8\text{Ag}_3\text{Sn}_2\text{Bi}_3\text{Cl}_{24}$, using PBE+SOC ϵ_{xc} functional.

Partial density of states (pDOS) plot, showing contribution of various orbitals in valence band maximum (VBM) and conduction band minimum (CBm) of few selected conformers

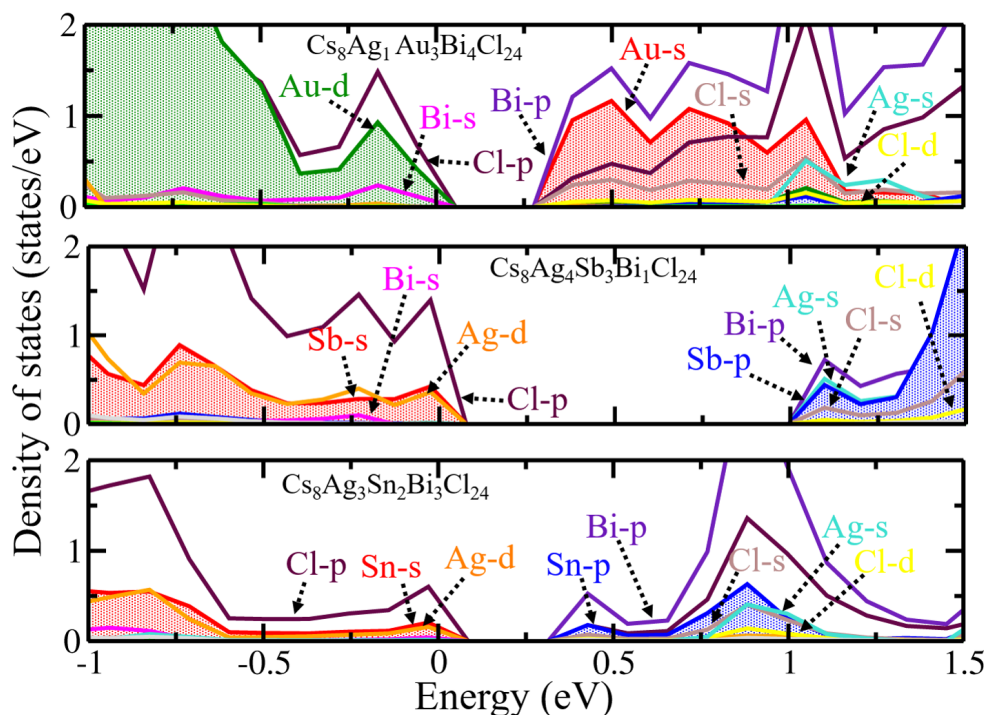


Figure 9: Partial density of states (pDOS) for $\text{Cs}_8\text{Ag}_1\text{Au}_3\text{Bi}_4\text{Cl}_{24}$, $\text{Cs}_8\text{Ag}_4\text{Sb}_3\text{Bi}_1\text{Cl}_{24}$ and $\text{Cs}_8\text{Ag}_3\text{Sn}_2\text{Bi}_3\text{Cl}_{24}$, using PBE+SOC ϵ_{xc} functional.

In Figure 9, through partial density of states (pDOS), we have presented a clear picture of different orbitals' contribution in VBM and CBm. We have noticed that molecular orbitals that contribute to VBM and CBm consist of hybridization of different atomic orbitals. Hence, complete substitution of Bi with Sb, eliminates the contribution of Bi s-orbital in CBm. As a consequence, the band gap increases. Similarly, in some cases, for 100% removal of Ag and Bi, a sudden change in band gap has been observed, which is ascribed to the elimination of non-degenerate energy levels.

Optical properties using HSE06 ϵ_{xc} functional

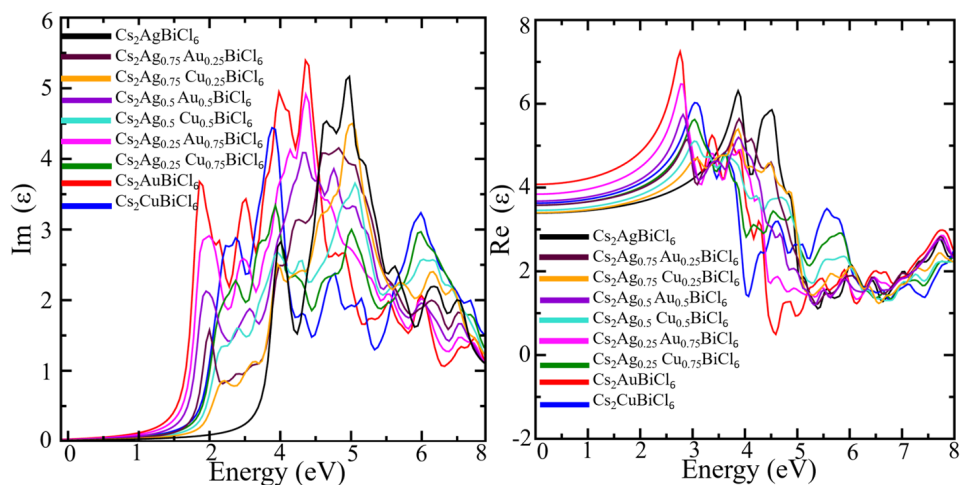


Figure 10: Variation of imaginary and real part of dielectric constant w.r.t. energy for double perovskites alloyed with monovalent cations, using HSE06 ϵ_{xc} functional.

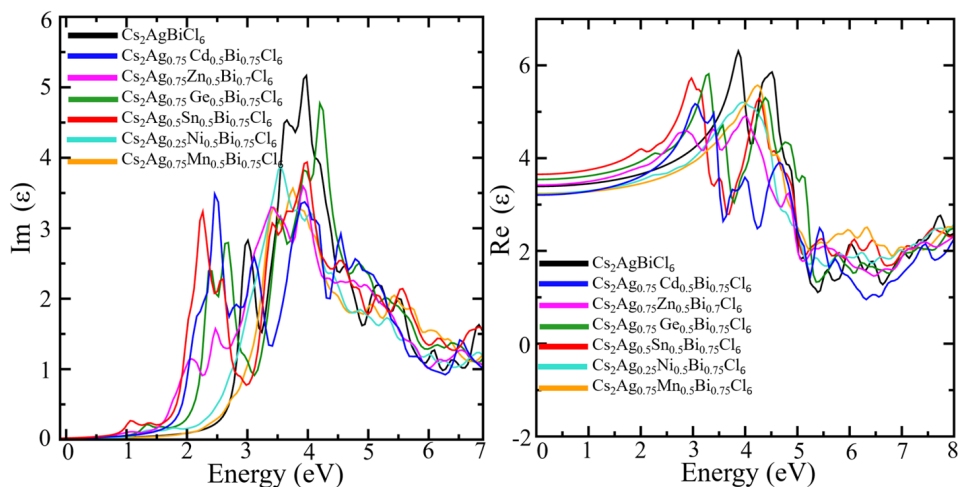


Figure 11: Variation of imaginary and real part of dielectric constant w.r.t. energy for double perovskites alloyed with divalent cations, using HSE06 ϵ_{xc} functional.

References

- (1) Frost, J. M.; Butler, K. T.; Brivio, F.; Hendon, C. H.; Van Schilfgaarde, M.; Walsh, A. Atomistic origins of high-performance in hybrid halide perovskite solar cells. *Nano*

- letters* **2014**, *14*, 2584–2590.
- (2) De Marco, N.; Zhou, H.; Chen, Q.; Sun, P.; Liu, Z.; Meng, L.; Yao, E.-P.; Liu, Y.; Schiffer, A.; Yang, Y. Guanidinium: a route to enhanced carrier lifetime and open-circuit voltage in hybrid perovskite solar cells. *Nano letters* **2016**, *16*, 1009–1016.
 - (3) Zhang, Y.; Liang, Y.; Wang, Y.; Guo, F.; Sun, L.; Xu, D. Planar FAPbBr₃ Solar Cells with Power Conversion Efficiency above 10%. *American Chemical Society Energy Letters* **2018**, *3*, 1808–1814.
 - (4) Kojima, A.; Teshima, K.; Shirai, Y. Tsutomu Miyasaka Organo metal Halide Perovskites as Visible-Light Sensitizers for Photovoltaic Cells. *Journal of the American Chemical Society* **2009**, *131*, 6050–6051.
 - (5) Savenije, T. J.; Ponseca, C. S.; Kunneman, L.; Abdellah, M.; Zheng, K.; Tian, Y.; Zhu, Q.; Canton, S. E.; Scheblykin, I. G.; Pullerits, T. et al. Thermally Activated Exciton Dissociation and Recombination Control the Carrier Dynamics in Organometal Halide Perovskite. *The Journal of Physical Chemistry Letters* **2014**, *5*, 2189–2194.
 - (6) Basera, P.; Kumar, M.; Saini, S.; Bhattacharya, S. Reducing lead toxicity in the methylammonium lead halide MAPbI₃: Why Sn substitution should be preferred to Pb vacancy for optimum solar cell efficiency. *Physical Review B* **2020**, *101*, 054108.
 - (7) Steirer, K. X.; Schulz, P.; Teeter, G.; Stevanovic, V.; Yang, M.; Zhu, K.; Berry, J. J. Defect Tolerance in Methylammonium Lead Triiodide Perovskite. *ACS Energy Letters* **2016**, *1*, 360–366.
 - (8) Yang, W. S.; Noh, J. H.; Jeon, N. J.; Kim, Y. C.; Ryu, S.; Seo, J.; Seok, S. I. High-performance photovoltaic perovskite layers fabricated through intramolecular exchange. *Science* **2015**, *348*, 1234–1237.

- (9) Huang, H.; Shi, J.; Zhu, L.; Li, D.; Luo, Y.; Meng, Q. Two-step ultrasonic spray deposition of $\text{CH}_3\text{NH}_3\text{PbI}_3$ for efficient and large-area perovskite solar cell. *Nano Energy* **2016**, *27*, 352–358.
- (10) Park, B.-w.; Seok, S. I. Intrinsic instability of inorganic–organic hybrid halide perovskite materials. *Advanced Materials* **2019**, *31*, 1805337.
- (11) Babayigit, A.; Ethirajan, A.; Muller, M.; Conings, B. Toxicity of organometal halide perovskite solar cells. *Nature Materials* **2016**, *15*, 247.
- (12) Kulbak, M.; Cahen, D.; Hodes, G. How important is the organic part of lead halide perovskite photovoltaic cells? Efficient CsPbBr_3 cells. *The Journal of Physical Chemistry Letters* **2015**, *6*, 2452–2456.
- (13) Liang, J.; Wang, C.; Wang, Y.; Xu, Z.; Lu, Z.; Ma, Y.; Zhu, H.; Hu, Y.; Xiao, C.; Yi, X. et al. All-inorganic perovskite solar cells. *Journal of the American Chemical Society* **2016**, *138*, 15829–15832.
- (14) Noel, N. K.; Stranks, S. D.; Abate, A.; Wehrenfennig, C.; Guarnera, S.; Haghighirad, A.-A.; Sadhanala, A.; Eperon, G. E.; Pathak, S. K.; Johnston, M. B. et al. Lead-free organic–inorganic tin halide perovskites for photovoltaic applications. *Energy & Environmental Science* **2014**, *7*, 3061–3068.
- (15) Hao, F.; Stoumpos, C. C.; Cao, D. H.; Chang, R. P.; Kanatzidis, M. G. Lead-free solid-state organic–inorganic halide perovskite solar cells. *Nature Photonics* **2014**, *8*, 489.
- (16) Filip, M. R.; Giustino, F. Computational screening of homovalent lead substitution in organic–inorganic halide perovskites. *The Journal of Physical Chemistry C* **2016**, *120*, 166–173.

- (17) Körbel, S.; Marques, M. A.; Botti, S. Stability and electronic properties of new inorganic perovskites from high-throughput ab initio calculations. *Journal of Materials Chemistry C* **2016**, *4*, 3157–3167.
- (18) Cai, Y.; Xie, W.; Teng, Y. T.; Harikesh, P.; Ghosh, B.; Huck, P.; Persson, K. A.; Mathews, N.; Mhaisalkar, S. G.; Sherburne, M. et al. High-throughput Computational Study of Halide Double Perovskite Inorganic Compounds. *Chemistry of Materials* **2019**, *31*, 5392–5401.
- (19) Chen, N.; Cai, T.; Li, W.; Hills-Kimball, K.; Yang, H.; Que, M.; Nagaoka, Y.; Liu, Z.; Yang, D.; Dong, A. et al. Yb-and Mn-Doped Lead-Free Double Perovskite Cs₂AgBiX₆ (X= Cl⁻, Br⁻) Nanocrystals. *American Chemical Society Applied Materials & Interfaces* **2019**, *11*, 16855–16863.
- (20) Slavney, A. H.; Hu, T.; Lindenberg, A. M.; Karunadasa, H. I. A bismuth-halide double perovskite with long carrier recombination lifetime for photovoltaic applications. *Journal of the American Chemical Society* **2016**, *138*, 2138–2141.
- (21) Volonakis, G.; Filip, M. R.; Haghighirad, A. A.; Sakai, N.; Wenger, B.; Snaith, H. J.; Giustino, F. Lead-free halide double perovskites via heterovalent substitution of noble metals. *The Journal of Physical Chemistry Letters* **2016**, *7*, 1254–1259.
- (22) Lamba, R. S.; Basera, P.; Bhattacharya, S.; Sapra, S. Band Gap Engineering in Cs₂(Na_xAg_{1-x})BiCl₆ Double Perovskite Nanocrystals. *The Journal of Physical Chemistry Letters* **2019**, *10*, 5173–5181.
- (23) Tran, T. T.; Panella, J. R.; Chamorro, J. R.; Morey, J. R.; McQueen, T. M. Designing indirect–direct bandgap transitions in double perovskites. *Materials Horizons* **2017**, *4*, 688–693.
- (24) Deng, W.; Deng, Z.-Y.; He, J.; Wang, M.; Chen, Z.-X.; Wei, S.-H.; Feng, H.-J. Synthesis of Cs₂AgSbCl₆ and improved optoelectronic properties of Cs₂AgSbCl₆/TiO₂ het-

- erostructure driven by the interface effect for lead-free double perovskites solar cells. *Applied Physics Letters* **2017**, *111*, 151602.
- (25) Volonakis, G.; Haghighirad, A. A.; Milot, R. L.; Sio, W. H.; Filip, M. R.; Wenger, B.; Johnston, M. B.; Herz, L. M.; Snaith, H. J.; Giustino, F. Cs₂InAgCl₆: a new lead-free halide double perovskite with direct band gap. *The Journal of Physical Chemistry Letters* **2017**, *8*, 772–778.
- (26) Locardi, F.; Cirignano, M.; Baranov, D.; Dang, Z.; Prato, M.; Drago, F.; Ferretti, M.; Pinchetti, V.; Fanciulli, M.; Brovelli, S. et al. Colloidal synthesis of double perovskite Cs₂AgInCl₆ and Mn-doped Cs₂AgInCl₆ nanocrystals. *Journal of the American Chemical Society* **2018**, *140*, 12989–12995.
- (27) Zhao, X.-G.; Yang, J.-H.; Fu, Y.; Yang, D.; Xu, Q.; Yu, L.; Wei, S.-H.; Zhang, L. Design of lead-free inorganic halide perovskites for solar cells via cation-transmutation. *Journal of the American Chemical Society* **2017**, *139*, 2630–2638.
- (28) Meng, W.; Wang, X.; Xiao, Z.; Wang, J.; Mitzi, D. B.; Yan, Y. Parity-forbidden transitions and their impact on the optical absorption properties of lead-free metal halide perovskites and double perovskites. *The Journal of Physical Chemistry Letters* **2017**, *8*, 2999–3007.
- (29) Perdew, J. P.; Chevary, J. A.; Vosko, S. H.; Jackson, K. A.; Pederson, M. R.; Singh, D. J.; Fiolhais, C. Atoms, molecules, solids, and surfaces: Applications of the generalized gradient approximation for exchange and correlation. *Physical Review B* **1992**, *46*, 6671.
- (30) Heyd, J.; Scuseria, G. E.; Ernzerhof, M. Hybrid functionals based on a screened Coulomb potential. *The Journal of Chemical Physics* **2003**, *118*, 8207–8215.
- (31) McClure, E. T.; Ball, M. R.; Windl, W.; Woodward, P. M. Cs₂AgBiX₆ (X= Br, Cl):

- new visible light absorbing, lead-free halide perovskite semiconductors. *Chemistry of Materials* **2016**, *28*, 1348–1354.
- (32) Kieslich, G.; Sun, S.; Cheetham, A. K. An extended tolerance factor approach for organic–inorganic perovskites. *Chemical science* **2015**, *6*, 3430–3433.
- (33) Li, C.; Lu, X.; Ding, W.; Feng, L.; Gao, Y.; Guo, Z. Formability of ABX_3 (X= F, Cl, Br, I) Halide Perovskites. *Acta Crystallographica Section B: Structural Science* **2008**, *64*, 702–707.
- (34) Kangsabanik, J.; Sugathan, V.; Yadav, A.; Yella, A.; Alam, A. Double perovskites overtaking the single perovskites: A set of new solar harvesting materials with much higher stability and efficiency. *Physical Review Materials* **2018**, *2*, 055401.
- (35) Sun, Q.; Chen, H.; Yin, W.-J. Do chalcogenide double perovskites work as solar cell absorbers: a first-principles study. *Chemistry of Materials* **2018**, *31*, 244–250.
- (36) Shockley, W.; Queisser, H. J. Detailed balance limit of efficiency of p-n junction solar cells. *Journal of Applied Physics* **1961**, *32*, 510–519.
- (37) Kumar, M.; Jain, M.; Singh, A.; Bhattacharya, S. Band gap Engineering by Sublattice Mixing in $Cs_2AgInCl_6$: High-throughput Screening from First-principles. *arXiv preprint arXiv:2004.07991* **2020**,
- (38) Savory, C. N.; Walsh, A.; Scanlon, D. O. Can Pb-free halide double perovskites support high-efficiency solar cells? *American Chemical Society Energy Letters* **2016**, *1*, 949–955.
- (39) Basera, P.; Saini, S.; Bhattacharya, S. Self energy and excitonic effect in (un)doped TiO_2 anatase: a comparative study of hybrid DFT, GW and BSE to explore optical properties. *Journal of Materials Chemistry C* **2019**, *7*, 14284–14293.

- (40) Yu, L.; Zunger, A. Identification of potential photovoltaic absorbers based on first-principles spectroscopic screening of materials. *Physical Review Letters* **2012**, *108*, 068701.
- (41) Jain, M.; Bhattacharya, S. Understanding the role of Sn substitution and Pb vacancy in FAPbBr₃ perovskites: A hybrid functional study. **2020, to be published**,
- (42) Filip, M. R.; Hillman, S.; Haghighirad, A. A.; Snaith, H. J.; Giustino, F. Band gaps of the lead-free halide double perovskites Cs₂BiAgCl₆ and Cs₂BiAgBr₆ from theory and experiment. *The Journal of Physical Chemistry Letters* **2016**, *7*, 2579–2585.
- (43) Hohenberg, P.; Kohn, W. Inhomogeneous electron gas. *Physical Review* **1964**, *136*, B864.
- (44) Kohn, W.; Sham, L. J. Self-consistent equations including exchange and correlation effects. *Physical Review* **1965**, *140*, A1133.
- (45) Blöchl, P. E. Projector augmented-wave method. *Physical Review B* **1994**, *50*, 17953.
- (46) Kresse, G.; Hafner, J. 14251); g. kresse, j. furthmüller. *Physical Review B* **1996**, *54*, 11169.
- (47) Pulay, P. Convergence acceleration of iterative sequences. The case of SCF iteration. *Chemical Physics Letters* **1980**, *73*, 393–398.
- (48) Monkhorst, H. J.; Pack, J. D. Special points for Brillouin-zone integrations. *Physical Review B* **1976**, *13*, 5188.